EFFECT OF SILICON ON ACTIVITY COEFFICIENTS OF P, BI, CD, SN, AND AG IN LIQUID Fe-Si, AND IMPLICATIONS FOR CORE FORMATION.

K. Righter[1], K. Pando[2], D.K. Ross[3], M. Righter[4], and T.J. Lapen[4] [1]NASA-JSC, Mailcode XI2, 2101 NASA Pkwy, Houston, TX 77058. [2]Jacobs JETS Contract, NASA-JSC, Houston, TX 77058, [3]Jacobs, NASA-JSC, Houston, TX 77058, [4]Dept. Earth, Atmospheric and Planetary Science, Univ. Houston, Houston, TX 77002

Introduction: Cores of differentiated bodies (Earth, Mars, Mercury, Moon, Vesta) contain light elements such as S, C, Si, and O. We have previously measured small effects of Si on Ni and Co [1,2], and larger effects on Mo, Ge, Sb, As [2] metal/silicate partitioning. The effect of Si on metal-silicate partitioning has been quantified for many siderophile elements [1,2,3], but there are a few key elements for which the effects are not yet quantified. Here we report new experiments designed to quantify the effect of Si on the partitioning of Bi, Cd, Sn, Ag, and P between metal and silicate melt. The results will be applied to Earth, Mars, Moon, and Vesta, for which we have good constraints on the mantle Bi, Cd, Sn, Ag, and P concentrations from mantle and/or basalt samples.

Experimental: Experiments were carried out using a piston cylinder apparatus and run conditions of 1 GPa and 1600 ºC. The starting materials comprised natural basaltic silicate (70% by mass) mixed with metallic Fe + 5% Bi and Cd or Sn and Ag (30% by mass). Silicon metal was also added to the metallic mixture at 2, 4, 6, and 10 %, to alloy with the Fe liquid and create an FeSi alloy of variable Si content. The MgO capsule reacted with the silicate melt to form more MgO-rich liquids that have 22-26 wt% MgO (Fig. 1).

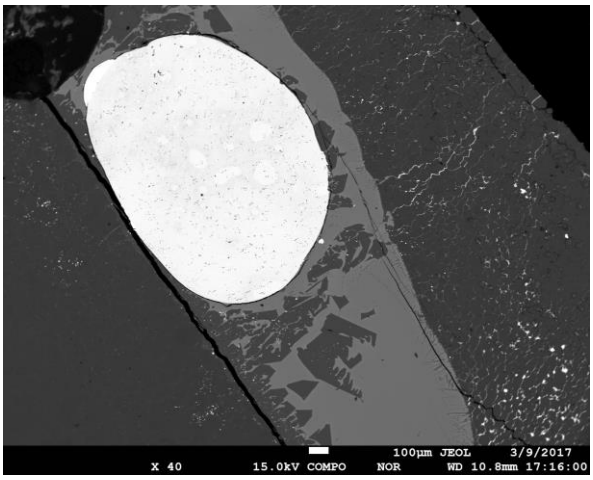

Figure 1: Experiment equilibrated at 1 GPa, 1600 ºC, with ~ 17 wt% Si in the metal. Bright rounded phase is Fe-Si-P-Bi-Cd alloy and light gray phase is silicate melt; some MgO capsule material (darkest phase) is also present in the silicate melt.

Analytical: Experimental metals (Fe, Bi, Cd, Sn, Ag, P, Si) and silicates (major elements) were analyzed using electron microprobe analysis (EMPA) at NASA-JSC utilizing a variety of mineral and glass standards with 15 kV and 20 nA conditions. Bi, Cd, Sn and Ag were measured in the silicate portion (most <100 ppm) using LA-ICP-MS (e.g., [2]) at the Univ. of Houston.

Results: The experimental results were used to calculate metal (met) - silicate (sil) exchange K_d according to this equation:

$MOn/2_{sil} + (n/2)Fe_{met} = M_{met} + (n/2)FeO_{sil}$ where n is the valence of the element M of interest. It can be shown that the slope of ln K_d versus ln(1-X_{Si}) gives ε_M^{Si} directly for each element [2], where ε_M^{Si} is an interaction parameter measuring the affinity of an element for FeSi liquids. Accordingly, interaction parameters are derived for Cd, Bi, Sn, Ag, and P in FeSi liquids (see [2], Fig. 2, Table 1). The interaction parameters for Fe-Si liquids are all positive and greater magnitude than those for Fe-S liquids, which are negative and smaller (Fig. 3). Interestingly, this means that any chalcophile behavior that may be exhibited by these elements during core formation will be muted or erased with even a

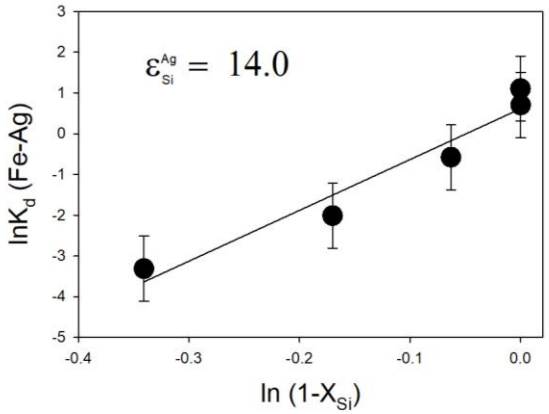

Figure 2: Correlation between Si content of the Fe metal and K_d(Ag-Fe) metal-silicate. Slope of the line yields the interaction parameter for Ag in FeSi liquids.

small amount of Si dissolved in the core-forming metallic liquid. Our results show that increasing Si causes a substantial increase in the activity coefficients (and corresponding decrease in partition coefficient) of all of these metals (Fig. 4). We will combine these results for Cd, Bi, Sn, Ag, and P with those for Fe-S and Fe-C

liquids [3,4] and apply the activity model to core formation in Earth, Mars and 4 Vesta.

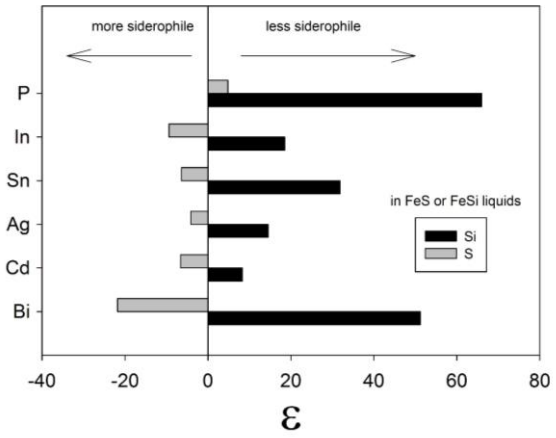

Figure 3: Comparison of our new results for P, In, Sn, Ag, Cd and Bi for Fe-Si interactions with those for Fe-S interaction from the literature [3,4].

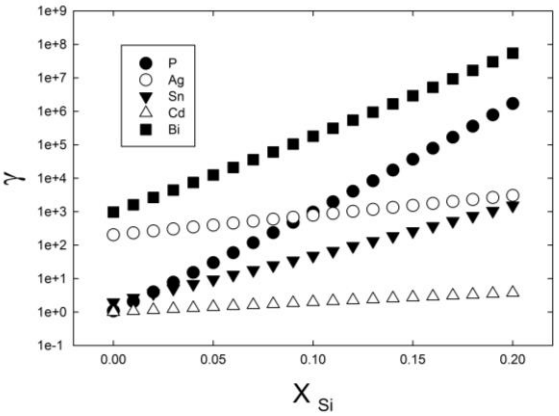

Figure 4: Activity coefficients of Sn, Ag, Cd and Bi in Fe-Si liquids with variable Si content of the FeSi liquid; temperature constant at 1600 ºC.

If a differentiated body is experiencing metallic core formation, the mantle concentration of each element (C^i_{LS}) can be calculated using the expression

$$C^i_{LS} = \frac{C^i_{bulk}}{x[p+(1-p)D^i_{SS/LS}]+(1-x)[D^i_{LM/LS}]}$$, where

$\ln D^i_{LM/LS}$ = alnfO$_2$ + b/T + cP/T + d(nbo/t) + e + lnγ(i)$_{met}$, constants a through e are derived by multiple linear regression of experimental data (Table 1), x is the fraction of silicate, p is the fraction of molten silicate, C^i_{bulk} is the bulk concentration of siderophile element, and $D^i_{SS/LS}$ is the partition coefficient between solid silicate and liquid silicate. Calculated Earth mantle [Sn] are shown for two accretion models– fixed and constant fO$_2$ (after [2]; Fig. 5). Mantle concentrations of all four elements can be explained by deep metal-silicate equilibrium, and thus do not require late addition of chondritic materials or a late veneer (e.g., 7,8]). Thus light elements can have a substantial influence on the evaluation of equilibrium partitioning between core and mantle and cannot be ignored.

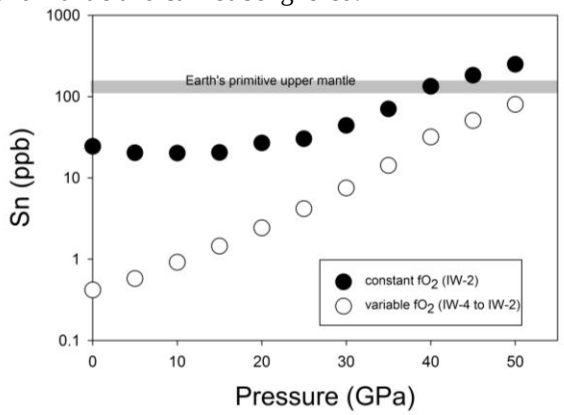

Figure 5: Variation of Sn content of the terrestrial mantle resulting from metal silicate equilibrium as the Earth accretes and pressure of metal-silicate equilibrium increases to 50 GPa (and 3800 K). At the high pressure conditions, D(Sn) becomes lower and Sn content matches that of the mantle (~ 140 ppm; [9]). D(Sn) data used in regression from [5,6, this study].

Table 1: Interaction parameters and regression coefficients

	Cd	**Bi**	**Sn**	**Ag**
ε_i^{Si}	+8.3	+51.2	+31.9	+14.2
a	-0.69	-0.49	-1.14	-0.087
b	-47400	-7173	-76870	+2002
c	+850	+1000	+1340	+200
d	+0.09	-0.12	-0.27	-0.58
e	9.8	8.46	20.64	8.53
n	42	24	104	58
r^2	0.87	0.81	0.84	0.86
2σ	0.72	1.25	1.71	0.69

References: [1] Tuff, J. et al. (2011) GCA 75, 673-690. [2] Righter, K. et al. (2017) GCA 198, 1-16. [3] Wood, B.J. et al. (2014) GCA 145, 248-267. [4] Lupis, C. (1983) Chem. Thermodyn. Materials, Elsevier, 581 pp. [5] Ballhaus, C. et al. (2017) CMP 172, 68. [6] Righter, K. et al. (2018) MaPS; in press; 10.1111/maps.13005. [7] Wang, Z., and Becker, H. (2013) Nature 499, 328-331. [8] Albarede, F. (2009) Nature 461, 1227-1233. [9] Palme, H. and O'Neill, H.St.C. (2014) Treat. Geoch. 2nd Ed., 1-39.